Ion Hydration Under Pressure: A Molecular Dynamics Study

Maksym Druchok and Myroslav Holovko

Institute for Condensed Matter Physics, Svientsitskii 1, 79011 Lviv, Ukraine

Reprint requests to M. H.; E-mail: holovko@icmp.lviv.ua

Z. Naturforsch. **68a,** 112 – 122 (2013) / DOI: 10.5560/ZNA.2012-0093
Received August 29, 2012 / published online February 15, 2013

It is a great honor for us to dedicate this paper to Professor Alfred Klemm on the occasion of his 100th birthday. M. Holovko remembers with pleasure his first meeting with Alfred Klemm during his first visit at the Max-Plank-Institut für Chemie in Mainz in 1986 together with Prof. Igor Yukhnovskii. They were invited to Klemm's house. It is nice to recall now these discussions on science, art, and literature.

This study is intended to elucidate the role of pressure on the hydration behaviour of ions in aqueous solutions. Molecular dynamics simulations were performed for systems modelling CsF, CsCl, CsBr, and CsI aqueous solutions under 'normal' (10^5 Pa, 298 K) and 'high pressure' ($4 \cdot 10^9$ Pa, 500 K) conditions. Structural details are discussed in terms of radial distributions functions, coordination numbers, and instantaneous configurations of the ionic hydration shells. The dynamic properties studied include the velocity autocorrelation functions and self-diffusion coefficients of the ions for both pressure regimes. The results indicate strong changes in the hydration behaviour and mobility of the ions.

Key words: High Pressure; Ion Hydration; Aqueous Electrolyte Solutions; Molecular Dynamics.

1. Introduction

The study of water and aqueous solutions under pressure is fundamentally important in many scientific areas, such as the geosciences, planetary modelling, and environmental sciences. At pressures between 0.1 and 10 GPa and temperatures between 300 and 500 K, liquid water is in equilibrium with several forms of ice, and its properties in this region differ from the ones under normal conditions. The effect of pressure on the structure of water has been a subject of a variety of experimental and theoretical investigations [1 – 8]. Since a pressure increase causes water to become denser than under normal conditions, this implies a disruption of the hydrogen-bond network.

Any change in the structure and hydrogen-bonding in water under pressure leads to a significant effect on the hydration in aqueous solutions. Sarma and Paul [9] performed a molecular dynamics (MD) study of the high pressure (0.8 GPa) effect on neopentane hydration and noticed an increase of hydration numbers and a reduction of hydrophobe association. One should also mention two recent investigations of the influence of pressure on ionic hydration by extended X-ray absorption fine structure (EXAFS) measurements for an RbBr aqueous solution under pressures up to 2.8 GPa [10] and for the hydration of Zn^{2+} in aqueous solutions under pressures up to 2.85 GPa (by means of EXAFS combined with MD simulations) [11]. These studies have shown structural changes in the ionic hydration shells, appearing in the ion–water radial distribution functions (RDFs) by a decrease of the height of the first peak and a shift toward smaller distances.

These conclusions are in agreement with older MD data for an aqueous solution of LiI at 0.3 GPa [12] and with our recent study of ion hydration for sodium halide aqueous solutions at 4 GPa and 500 K [13]. Among the ions considered, the most dramatic pressure effect on the hydration structure is observed for Br^- and I^- anions, while the octahedral structure of Zn^{2+} remains unchanged [11]. Weakly influenced hydration shells were also found for Na^+ and F^- ions [13]. Therefore the hydration structure can be stable under pressure not only for cations but also for anions with relatively small sizes. These differences find their origin in the different strength of the ion–

water electrostatic interaction acting as stabilization factor [14]. A large size of the ion and/or a small charge are the factors decreasing the ion–water electrostatic interactions. Due to this the hydration shells of Cl^-, Br^-, and I^- anions can be highly affected by a high pressure. In contrast to these anions, the cations such as Na^+, Li^+, and Zn^{2+}, and the F^- anion are characterized by smaller sizes and highly stable hydration shells.

In this paper, we show that a significant pressure influence on the hydration structure can be also observed for large cations like Cs^+. For this aim, a series of aqueous solutions is considered: CsF, CsCl, CsBr, and CsI. For these solutions a set of all-atom MD simulations was performed in the NpT ensemble to reveal their properties under 'normal' (10^5 Pa, 298 K) and 'high pressure' ($4 \cdot 10^9$ Pa, 500 K) conditions. We denote 'normal pressure' regime by NP and 'high pressure' by HP. In our previous study [13] of the pressure influence on the hydration behaviour in sodium halide solutions, the same NP and HP regimes were considered. For the HP regime, we increased the temperature to avoid transition to a solid phase (in pure water: ice VI for a pressure of 1 – 2 GPa or ice VII for higher pressures).

Similar to [13], we focus on the influence of pressure on the ion–water (ion–oxygen and ion–hydrogen) RDFs and the corresponding running coordination numbers. Besides the structural changes, we also discuss changes of the dynamic properties in terms of the velocity autocorrelation functions and the self-diffusion coefficients of the ions.

2. Model and Method

The MD simulations were performed with the standard DL_POLY package [15]. Pressure and temperature were controlled by means of a Nose–Hoover barostat and thermostat [16, 17]. The MD unit cells with periodic boundary conditions contained 2352 water molecules, 12 anions (F^-, Cl^-, Br^-, or I^-), and 12 Cs^+ cations. All species were allowed to move freely across the MD cell. At normal pressure the electrolyte concentration is ≈ 0.28 mol/l, at high pressure regime, the unit cell is more compact, and the electrolyte concentration rises to ≈ 0.40 mol/l. Water–water, ion–water, and ion–ion interactions $U_{ij}(r)$ consist of the long-range Coulomb contribution and a short-range one, modelled by the Lennard–Jones potential

$$U_{ij}(r) = \frac{Z_i Z_j e_0^2}{4\pi\varepsilon_0 r} + 4\varepsilon_{ij}\left[(\sigma_{ij}/r)^{12} - (\sigma_{ij}/r)^6\right], \qquad (1)$$

where the symbols have their conventional meanings.

Ion specific effects in electrolyte solutions are often investigated for a series of monovalent anions and cations. Having ions with the same charge but different sizes reveals significant differences in solvation, which is a key feature for the structural and dynamic properties. In [18], Koneshan et al. performed MD simulations of a series of aqueous solutions of F, Cl, Br, I, Li, Na, K, Rb, Cs, Ca ions described with Dang's parameter set [19 – 26]. The studies have shown a significant dependence of ion mobility on size. Fennel et al. tested parameter sets by Dang, Jorgensen [27], and Jensen and Jorgensen [28] for the alkali halides and noted size-dependent ion pairing effects [29]. This is in accord with recent observations about the binding of like-ions via bridging water molecules [30, 31].

In this study, we use Dang's set of parameters for the CsX ion pairs. Water is described by the simple point charge-extended (SPC/E) model [32]. In this model, the effective charges $Z_H e_0 = 0.4238 \cdot e_0$ and $Z_O = -2Z_H$ are assigned to hydrogen and oxygen atoms (e_0 is the elementary electric charge).

The charges and Lennard–Jones parameters (σ_i, ε_i) are collected in Table 1. The mixing rules for the Lennard–Jones parameters are

$$\begin{aligned} \sigma_{ij} &= (\sigma_i + \sigma_j)/2\,, \\ \varepsilon_{ij} &= \sqrt{\varepsilon_i \varepsilon_j}\,. \end{aligned} \qquad (2)$$

Every solution was equilibrated during 10^6 steps, and the production runs were performed over 10^7 steps. We used the velocity Verlet algorithm with a time step of $\tau = 5 \cdot 10^{-16}$ s to integrate the classical equations

Table 1. Interaction parameters, see (1) and (2).

	species	Z_i	ε_i (kcal/mol)	σ_i (Å)
water	O	−0.8476	0.1554	3.1656
	H	0.4238	0.0	0.0
electrolyte	Cs	1.00	0.1000	3.8865
	F	−1.00	0.1799	3.1205
	Cl	−1.00	0.1000	4.4045
	Br	−1.00	0.1000	4.6265
	I	−1.00	1.0000	5.1705

of motion. The long-range Coulomb interactions were treated with the Ewald summation technique.

To quantify the structural differences in the hydration of the ions under NP and HP conditions, we present the ion–oxygen and ion–hydrogen RDFs $g_{\mathrm{XO}}(r)$, $g_{\mathrm{XH}}(r)$, the corresponding running coordination numbers $n_{\mathrm{XO}}(r)$, $n_{\mathrm{XH}}(r)$ and accompany them with instantaneous configurations. The function describing the running coordination numbers, $n_{\alpha\beta}(r)$, is defined as the number of particles β in a sphere of radius r around a particle α in the center:

$$n_{\alpha\beta}(r) = 4\pi\rho_\beta \int_0^r g_{\alpha\beta}(\lambda)\lambda^2\,\mathrm{d}\lambda\,, \tag{3}$$

where ρ_β is the number density of species β in the system. Hydration is often characterized by the coordination number $n_{\alpha\mathrm{O}}(r_{\min})$, which corresponds to the average number of water molecules in the first hydration shell of an α particle. $r_{\min}$ is the position of the first minimum in the RDF, which is taken as the boundary of the hydration shell.

Dynamic properties are considered in terms of normalized velocity autocorrelation functions (VACFs):

$$\Psi_\alpha(t) = \frac{\left\langle \overrightarrow{v}_\alpha(0)\overrightarrow{v}_\alpha(t)\right\rangle}{\left\langle \overrightarrow{v}_\alpha(0)\overrightarrow{v}_\alpha(0)\right\rangle}\,, \tag{4}$$

where $\overrightarrow{v}_\alpha(t)$ is the velocity vector of all particles of species $\alpha = \mathrm{Cs/F/Cl/Br/I}$ at time t and $\langle\ \rangle$ denotes the thermodynamic equilibrium average.

The corresponding self-diffusion coefficients have been also calculated by integrating the VACFs in accordance with the Green–Kubo relation:

$$D_\alpha = \frac{1}{3N_\alpha}\int_0^\infty \left\langle \overrightarrow{v}_\alpha(0)\overrightarrow{v}_\alpha(t)\right\rangle \mathrm{d}t\,, \tag{5}$$

where N_α is the number of particles α and $t = 25$ ps is taken as the limit (∞) since the correlation functions have completely decayed at this time.

3. Results and Discussion

In this section, we show selected results from the simulations. The structural results have been collected in Figures 1–6 and Table 2. They indicate an overall strong pressure impact on the hydration structure of the ions.

First we consider the cesium–water correlations. The Cs–O and Cs–H RDFs for all solutions behave in the same way, we shall thus discuss them for CsF only. Figure 1 presents these RDFs, the coordination numbers, and instantaneous configurations of the cesium hydration shell. The Cs–O RDF (Fig. 1, top left) shows a small shift of the first peak position when going from NP to HP, while the height remains unchanged. Higher-order peaks, however, do not coincide in the NP and HP cases: the hydration of cesium at the HP point demonstrates a more pronounced correlation at larger distances. Despite the visually similar Cs–O first peaks the coordination numbers are higher in the HP case because of the higher density: $n_{\mathrm{CsO}}(r_{\mathrm{min1}}) \approx 9$ in NP vs. ≈ 14 in the HP case. The Cs–H RDFs show larger differences between the NP and HP cases: the first peak shifts toward smaller distances and the height decreases. As above, in the HP case one sees RDF oscillations at larger distances, while the running coordination numbers reflect a more packed structure. The hydrogen coordination numbers for the different solutions increase from $\approx 25-26$ to $\approx 33-34$ when going from NP to HP.

In Figure 1, instantaneous configurations (all water molecules with oxygens within a sphere of the radius r_{min1} around the ion) of first hydration shells of Cs^+ under normal (bottom left plot, $r_{\mathrm{min1}} = 4.03$ Å) and high (bottom right plot, $r_{\mathrm{min1}} = 4.20$ Å) pressures are also shown. It can be seen that the hydration shell becomes markedly more crowded at high pressure.

Table 2. Structural properties of ionic hydration.

	NP		HP	
ionic pair	r_{min1} [Å]	$n(r_{\mathrm{min1}})$	r_{min1} [Å]	$n(r_{\mathrm{min1}})$
in CsF solution				
Cs-O	4.03	9.2	4.20	14.3
Cs-H	4.69	26.7	4.54	33.8
F-O	3.28	6.4	3.32	7.8
F-H	2.47	6.4	2.42	7.1
in CsCl solution				
Cs-O	4.03	8.8	4.19	14.0
Cs-H	4.70	25.9	4.55	33.5
Cl-O	3.90	7.1	4.48	16.3
Cl-H	3.05	6.7	2.85	7.6
in CsBr solution				
Cs-O	4.03	8.8	4.19	14.0
Cs-H	4.70	25.9	4.55	33.5
Br-O	4.00	7.2	4.59	17.5
Br-H	3.14	6.8	2.93	7.6
in CsI solution				
Cs-O	4.02	8.5	4.19	13.9
Cs-H	4.70	25.3	4.55	33.2
I-O	4.26	7.5	4.90	20.8
I-H	3.41	6.8	3.12	7.4

From Table 2 one sees a general trend to a slight monotonic reduction of the Cs–O and Cs–H hydration numbers along the series of solutions: CsF, CsCl, CsBr, CsI.

Next we consider the influence of pressure on the hydration of the fluorine ion. The changes of RDFs, coordination numbers, and instantaneous configurations of the first hydration shell are presented in Figure 2. The first peaks of the F–O and F–H RDFs experience a height decrease and a slight shift to smaller separations when the pressure is increased. The second peaks become less pronounced and so do the long distance oscillations. The analysis of the mean coordination numbers for F–O and F–H shows that additional water molecules enter the fluoride's first hydration shell (from ≈ 6.4 oxygens to ≈ 7.8, from ≈ 6.4 hydrogens to ≈ 7.1). One can explain this weak increase, in contrast to the cesium hydration, by the relatively small size of the F^- ion and therefore by a strong hydration preventing new neighbours from entering the hydration shell. For a better illustration, we show snapshots of the F^- first hydration shell under NP and HP conditions (bottom left and right plots in Fig. 2, respectively). One sees that under the high pressure the octahedral arrangement of the water molecules around the ion is lost and that eight neighbours form a more complicated and compact structure.

For chlorine ions: they are characterized by a larger size than F^-, so one can expect the water molecules in

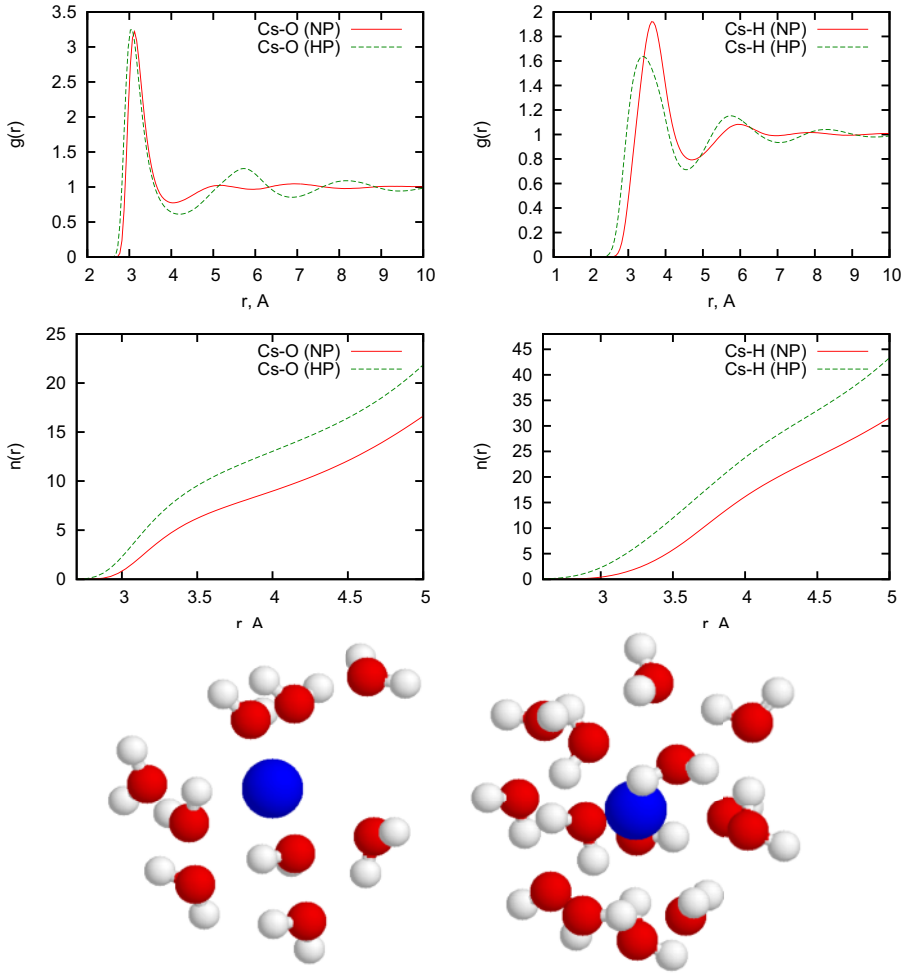

Fig. 1 (colour online). Cs–O and Cs–H RDFs (top), running coordination numbers (center), and instantaneous configurations of a Cs^+-hydration shell (water molecules with oxygens inside of sphere of radius $r_{\min 1}$ around the ion) under normal (bottom left, $r_{\min 1} = 4.03$ Å) and high (bottom right, $r_{\min 1} = 4.20$ Å) pressures in a CsF solution.

the chlorine hydration shell to be bound more weakly. In Figure 3, we present the Cl–O and Cl–H RDFs, the corresponding coordination numbers, and instantaneous configurations. The first peak of the Cl–O RDF shifts to smaller r and decreases its height, but significantly extends its range when the pressure is increased: in the NP case, the location of the first minimum is 3.9 Å, while in the HP case it is $\approx$ 4.5 Å. Similar to the Cs case, in the HP regime the Cl–O RDF has oscillations at larger distances. The Cl–H first peak becomes lower and shifts toward smaller distances, the second peak is also displaced in the same direction. The mean Cl–O coordination number increases from $\approx$ 7.1 to $\approx$ 16.3. Clearly the hydration shell of the Cl^- ion demonstrates weaker binding than in the fluoride case and allows more new neighbours to approach the ion in the HP regime. The mean Cl–H coordination number shows a very small increment from $\approx$ 6.7 to 7.6. The instantaneous configurations of the chloride first hydration shells under normal and high pressures are shown in the bottom plots of Figure 3.

The Br–O and Br–H RDFs, the running coordination numbers, and snapshots are presented in Figure 4. Since Br^- and Cl^- ions are close in sizes, one sees a similarity with the Cl case. The first peak of the Br–O distribution widens in the HP regime, its maximum position shifts to smaller distances, while the mini-

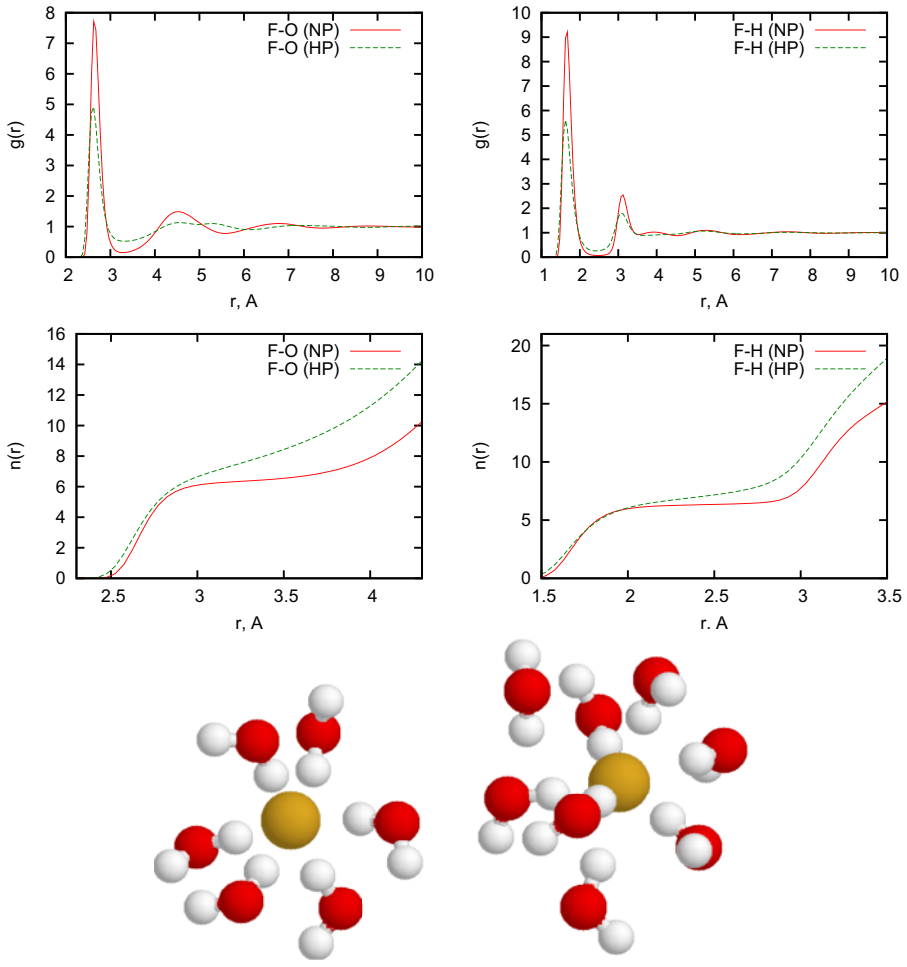

Fig. 2 (colour online). F–O and F–H RDFs (top), running coordination numbers (center), and instantaneous configurations of an F^- ion hydration shell (water molecules inside of a sphere of radius $r_{\min 1}$ around the ion) under normal (bottom left, $r_{\min 1} = 3.28$ Å) and high (bottom right, $r_{\min 1} = 3.32$ Å) pressures in a CsF solution.

mum moves from 4.0 Å to 4.6 Å. In the HP case the Br–O distribution also demonstrates long-distance oscillations. The mean number of neighbouring oxygens (as defined by the position of first Br–O minimum) increases from 7.2 to 17.5. The first Br–H peak slightly shifts to smaller distances and the average number of neighbouring hydrogens rises from 6.8 to 7.6.

Next we explore the hydration of the iodine ion. In Figure 5, the pressure influence on the iodide hydration shell is shown. Iodide is the largest of the ions considered here, and one can expect the most pronounced changes in its hydration shell. Indeed, the mean number of oxygens in its hydration shell increases from 7.5 to 20.8. The first peak of the I–O RDF even slightly increases its height in the HP case and shifts its maximum toward smaller separations. The position of first minimum changes to larger r from 4.3 to 4.9 Å, the I–O distribution also demonstrates longer oscillations in the HP regime. The I–H RDF reveals the same trends as found before for other anion–hydrogen distributions. The average number of neighbouring hydrogens around the iodine ion increases from 6.8 to 7.4.

Note that the ion–oxygen and the ion–hydrogen coordination numbers increase to a different degree due to the NP–HP transition. This is because of the dif-

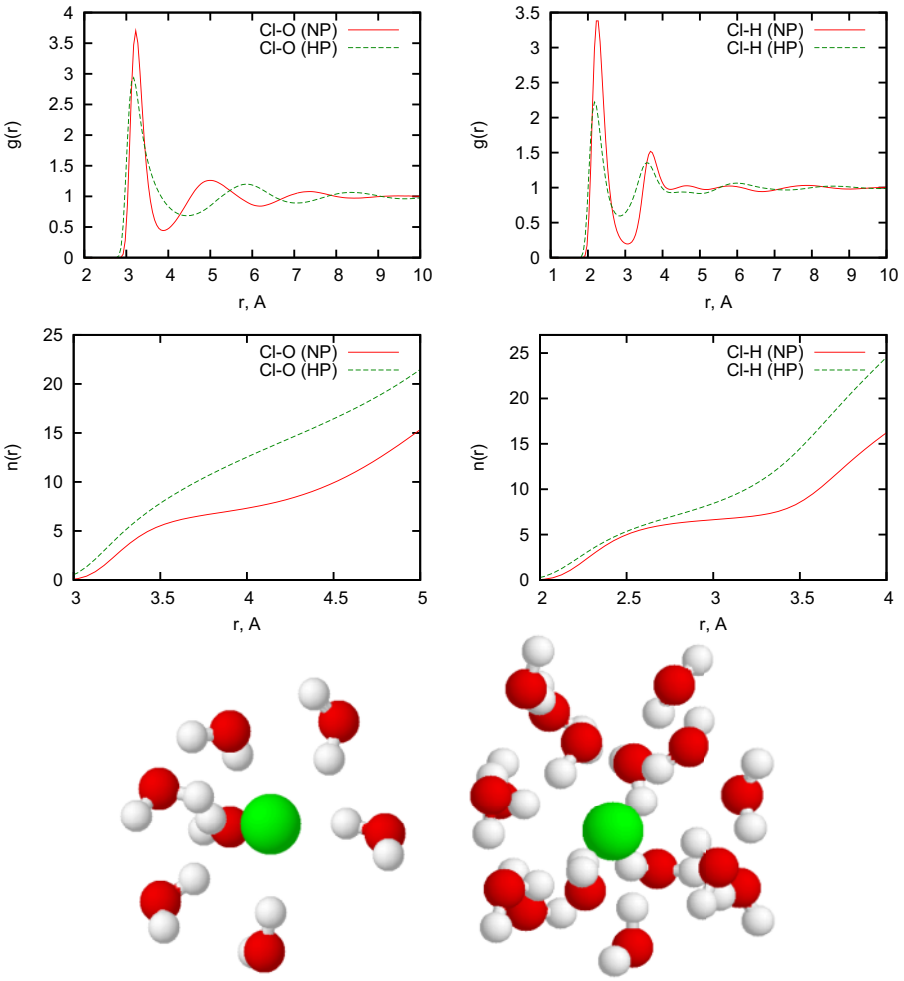

Fig. 3 (colour online). Cl–O and Cl–H RDFs (top), running coordination numbers (center), and instantaneous configurations of a Cl^- hydration shell (water molecules inside of a sphere of radius $r_{min\,1}$ around the ion) under normal (bottom left, $r_{min\,1} = 3.90$ Å) and high (bottom right, $r_{min\,1} = 4.48$ Å) pressures in CsCl solution.

ferent ability of the ions to accommodate new neighbours and then to reorder their hydration shells. Thus in addition to the RDFs and coordination numbers, we have studied the pressure effect on an angle distribution characterizing the orientation of the hydrating water molecules. For this purpose, we monitored the angle between the water molecule dipole moments and the oxygen–ion directions and built the corresponding distributions for all ions in the NP and HP regimes. In Figure 6, these distributions $P(\alpha)$ are presented.

One clearly sees that in the NP case all anion hydration shells show a single maximum at $\alpha \approx 54^\circ$. This angle corresponds to the orientation when a water molecule points one of its hydrogen atoms toward the anion. The tiny peaks at $\alpha \approx 0^\circ$ and the shoulder at $100-160^\circ$ we ascribe to water molecules approaching the anionic hydration shells from the bulk. In the series from F^- to I^- the peaks at 54° become lower. This is in accord with our previous finding about the 'strict' hydration of the fluoride ions and a more 'loose' one of the larger anions. The wide distribution for the Cs^+ case shows a maximum at about 120°. This is also in agreement with our previous observations, which reported a loosely-oriented hydration of the Cs^+ ions.

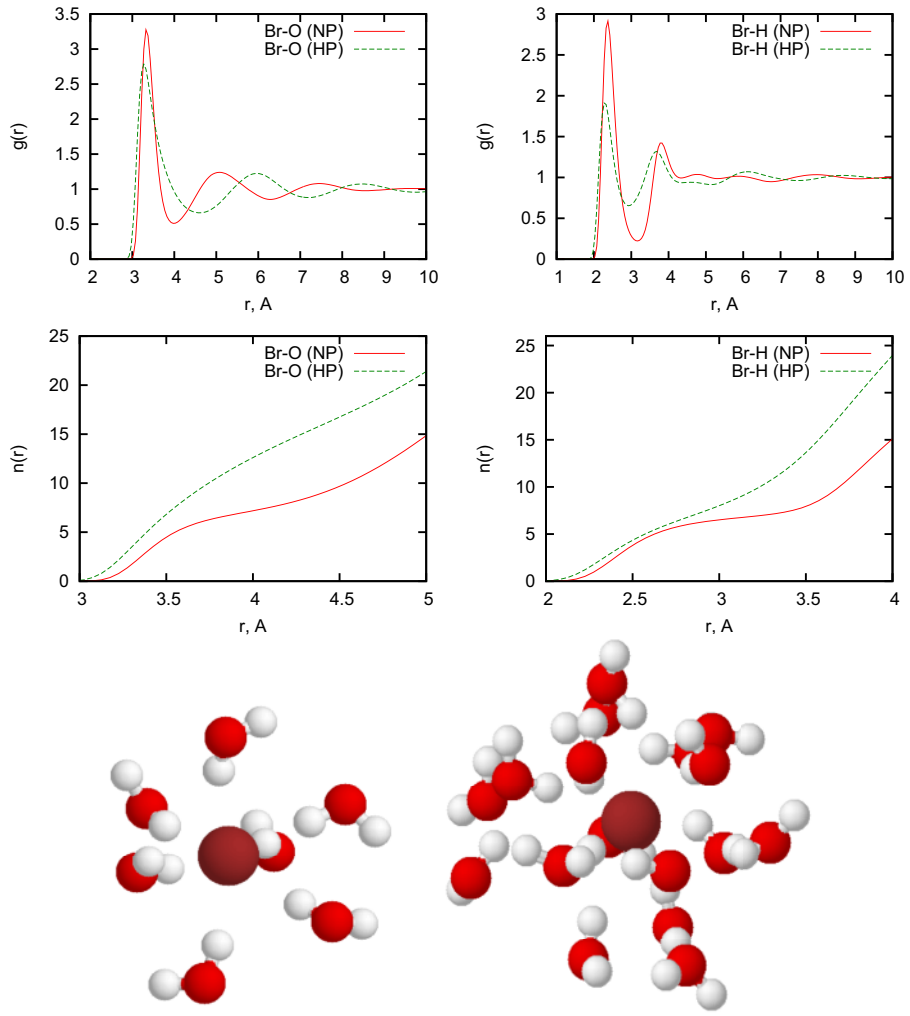

Fig. 4 (colour online). Br–O and Br–H RDFs (top), running coordination numbers (center), and instantaneous configurations a Br^- hydration shell (water molecules inside of a sphere of radius r_{min1} around the ion) under normal (bottom left, $r_{min1} = 4.00$ Å) and high (bottom right, $r_{min1} = 4.59$ Å) pressures in CsBr solution.

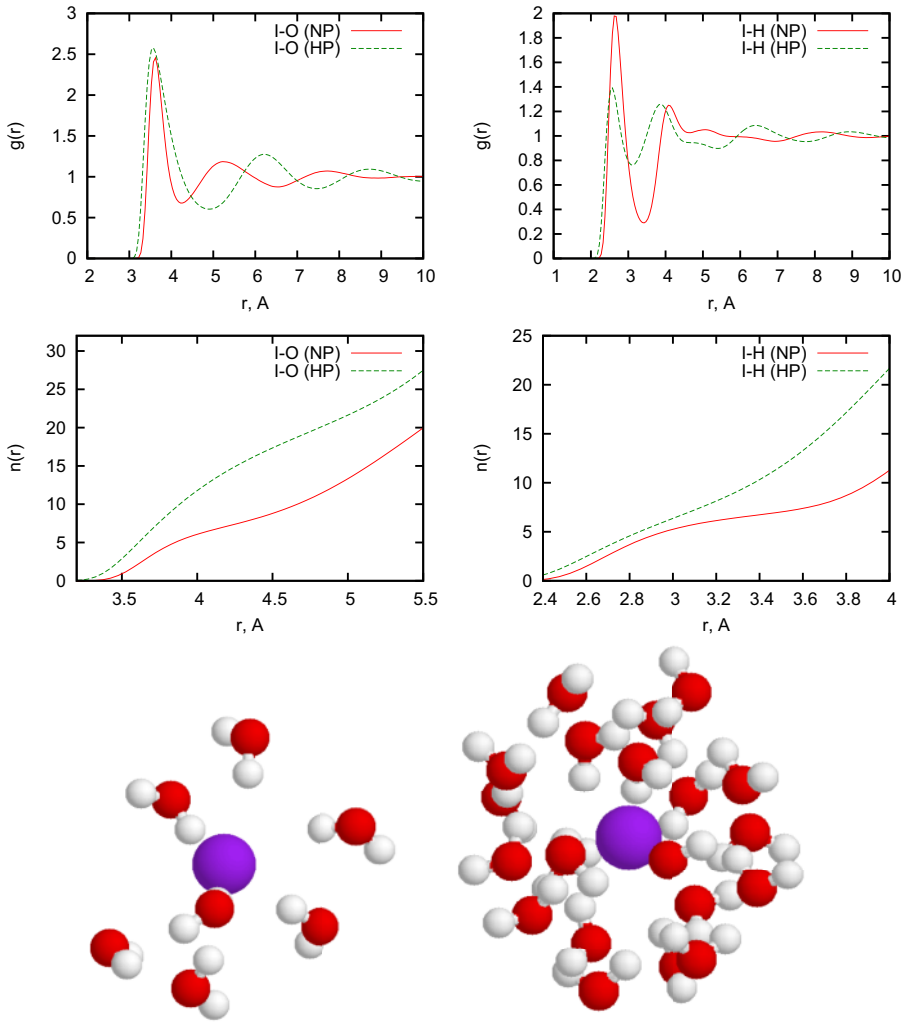

Fig. 5 (colour online). I–O and I–H RDFs (top), running coordination numbers (center), and instantaneous configurations of an I^- hydration shell (water molecules inside of a sphere of radius r_{min1} around the ion) under normal (bottom left, $r_{min1} = 4.26$ Å) and high (bottom right, $r_{min1} = 4.90$ Å) pressures in CsI solution.

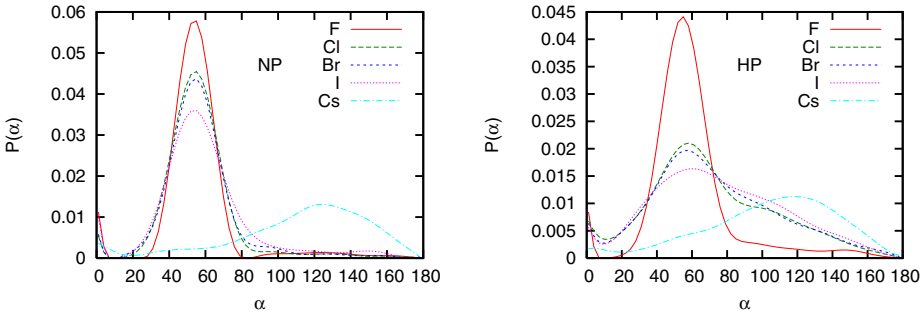

Fig. 6 (colour online). Distributions of the angles α between the dipole moment of the water molecules in the ionic hydration shells and the oxygen–ion direction. NP: left panel, HP: right panel.

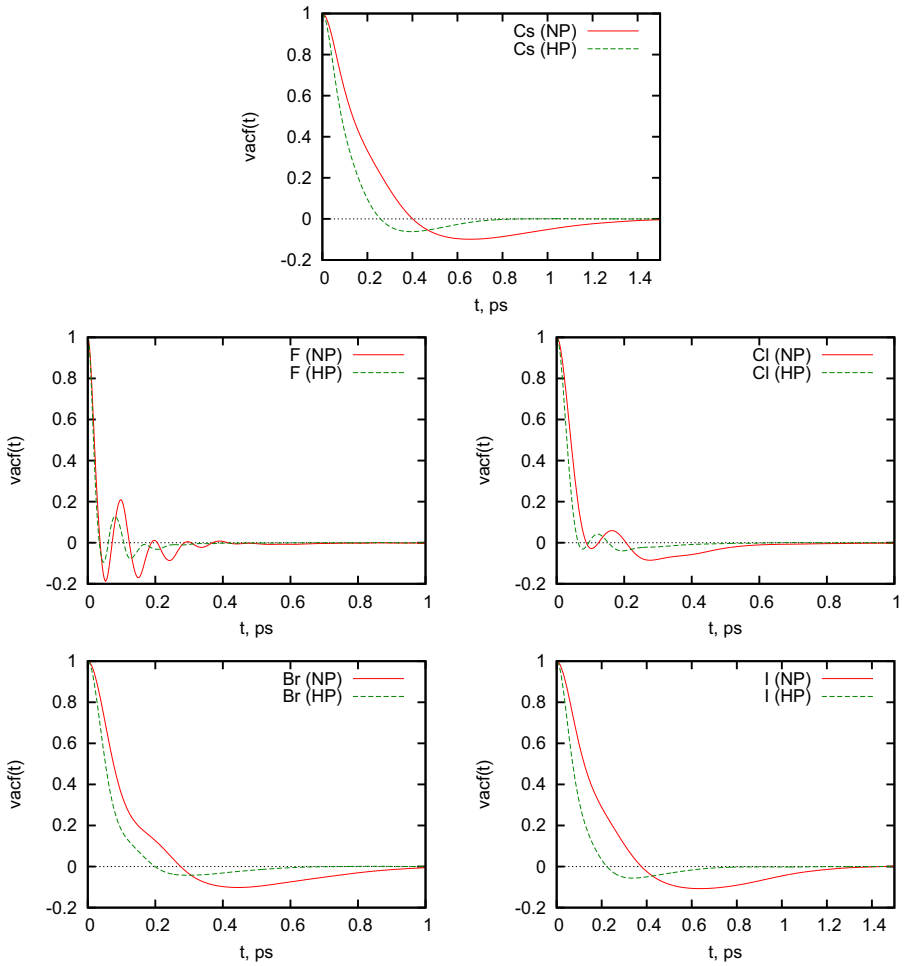

Fig. 7 (colour online). Normalized VACFs of Cs^+, F^-, Cl^-, Br^-, and I^- ions in the normal and high pressure regimes. The cesium VACF is the one from the CsF solution.

One might expect that the pressure transition would affect the angle distribution around this ion, which experiences a significant change in the number of neighbours. However, this as well as the F^--distribution do not evolve much when the pressure is increased. The latter one does not change its distribution since the hydration structure does not allow new water molecules to accommodate, while the first one is characterized by a loosely oriented hydration shell already in the NP regime. This is not the case for Cl^-, Br^-, and I^- ions: in the HP case, the main peaks at 54° become wider, lower, and asymmetric since new water molecules enter the hydration shells.

We also explored dynamic properties of the ions in terms of the normalized velocity autocorrelation functions and the self-diffusion coefficients in both pressure regimes. Plots of the normalized velocity autocorrelation functions have been collected in Figure 7.

The cesium VACF under NP conditions shows a regular shape for a diffusive particle with a single backscattering oscillation. One might expect that the increase of pressure would lead to a faster decay of the velocity correlation. Indeed in the HP case, the shape does not change, however the position of the minimum is displaced from 0.65 to 0.4 ps, the correlation decays faster. In contrast to the cesium case, the fluoride VACF in the NP regime shows several oscillations in the region 0 – 0.4 ps. The oscillations of the corresponding HP-VACF are characterized by a shorter period, a weaker magnitude, and a faster decay. Such an oscil-

Table 3. Self-diffusion coefficients D of the ions (in 10^{-9} m^2/s).

ion	NP	HP
	in CsF solution	
Cs	1.83	2.49
F	1.00	2.90
	in CsCl solution	
Cs	1.87	2.55
Cl	1.52	2.90
	in CsBr solution	
Cs	1.95	2.54
Br	1.57	2.85
	in CsI solution	
Cs	1.94	2.37
I	1.64	2.22

lating behaviour is a consequence of the tight hydration of the F-ion (cage effect of the hydration shell). In the series Cl→Br→I, this cage effect is weakened and the shapes of the VACFs evolve toward the one observed for cesium. The large, loosely hydrated, and heavy iodine ion is weakly affected by the solution, so it has the longest velocity correlation. The pressure effect along the series follows the pattern observed above.

The self-diffusion coefficients have been collected in Table 3. First we consider them for the anions in the NP regime; they slightly increase in the direction from fluoride to iodide solutions. The explanation for this can again be found in the different ionic hydration: more loosely hydrated ions are more mobile. The cesium coefficient increases in the same direction, which may imply a certain degree of association with the anions. The self-diffusion coefficients reported by Koneshan et al. [18] are in good agreement with our results, but one should bear in mind that this study considered ions at infinite dilution and neglected ion–ion interactions.

What happens when pressure and temperature of an aqueous solution increase? High pressure has a twofold impact – a denser system slows down the ions, but also initiates a process of orientational rearrangements in the hydration shell of Cl^-, Br^-, and I^- ions from a more oriented order at NP to a looser ordering at HP. Such a loose hydration decreases the effective mass of the ions, thus increasing their mobility. The other factor mobilizing the ions is the high temperature, without which these systems cannot exist in the liquid state. Similar trends were observed for sodium halides solutions [13].

4. Summary and Conclusions

In this article, we discussed results of molecular dynamics study of the influence of pressure ion the hydration of cesium halides. Two pressure regimes are considered: i) normal – 0.1 MPa, 298 K and ii) high – 4 GPa, 500 K. It is found that the transition from the normal to the high pressure regime influences the structural and dynamic properties of ions on a different scale. The hydration numbers of the F^--ion, $n_{FO}(r_{min1})$ and $n_{FH}(r_{min1})$, change only little. This is due to the strong fluoride hydration, preventing new neighbours from entering the hydration shell. For a series of larger ions, Cl^-, Br^-, and I^-, we have observed a weak increase of hydrogen neighbours, while the anion–oxygen coordination numbers grow markedly. In contrast to the previously observed behaviour of the Na–O coordination number, which is only weakly affected by the pressure factor [13], $n_{CsO}(r_{min1})$ is much more sensitive, and so is $n_{CsH}(r_{min1})$.

We have also analyzed the pressure influence on the dynamic properties of the ions in terms of velocity autocorrelation functions and self-diffusion coefficients. One might expect that the HP regime would slow down the ions, but we see that the ionic self-diffusion coefficients increase. Such a rise of the ionic mobilities is due to their loose hydration (the effective ionic mass is lowered) and to the higher temperature (500 K in HP vs. 298 K in NP case), which speeds up the particles. The self-diffusion coefficient of the Cs^+-ion shows a slight dependence on the type of the counter-anion.

Acknowledgements

We thank Prof. Philippe Bopp for his interest in this study and useful discussions.

[1] M.-C. Bellissent-Funel and L. Bosio, J. Chem. Phys. **102**, 3727 (1995).
[2] K. Bagchi, S. Balasubramanian, and M. L. Klein, J. Chem. Phys. **107**, 8561 (1997).
[3] A. G. Kalinichev, Y. E. Gorbaty, and A. V. Okhulkov, J. Mol. Liq. **82**, 57 (1999).
[4] A. K. Soper and M. A. Ricci, Phys. Rev. Lett. **84**, 2881 (2000).

[5] E. Schwegler, G. Galli, and F. Gygi, Phys. Rev. Lett. **84**, 2429 (2000).
[6] J. H. Eggert, G. Weck, and P. Loubeyre, J. Phys. Condens. Matter. **14**, 11385 (2002).
[7] A. M. Saitta and F. Datchi, Phys. Rev. E. **67**, 20201 (2003).
[8] T. Strässle, A. M. Saitta, Y. Le Godec, G. Hamel, S. Klotz, J. S. Loveday, and R. J. Nelmes, Phys. Rev. Lett. **96**, 67801 (2006).
[9] R. Sarma and S. Paul, J. Chem. Phys. **136**, 114510 (2012).
[10] A. Filipponi, S. De Panfilis, C. Oliva, M. A. Ricci, P. D' Angelo, and D. T. Bowron, Phys. Rev. Lett. **91**, 165505 (2003).
[11] V. Migliorati, G. Chillemi, G. Mancini, A. Zitolo, S. Tatoli, A. Filipponi, and P. D'Angelo, J. Phys. Conf. Ser. **190**, 012057 (2009).
[12] G. J. Szász and K. Heinzinger, Sci. Lett. **64**, 163 (1984).
[13] M. Druchok and M. Holovko, J. Mol. Liq. **159**, 24 (2011).
[14] M. Holovko, M. Druchok, and T. Bryk, J. Chem. Phys. **123**, 154505 (2005).
[15] http://www.ccp5.ac.uk/DL_POLY_CLASSIC/.
[16] J. M. Hayle, Molecular Dynamics Simulations: Elementary Methods, Wiley, New York 1992.
[17] S. Melchionna, G. Ciccotti, and B. L. Holian, Molec. Phys. **78**, 533 (1993).
[18] S. Koneshan, J. C. Rasaiah, R. M. Lynden-Bell, and S. H. Lee, J. Phys. Chem. B **102**, 4193 (1998).
[19] L. X. Dang, Chem. Phys. Lett. **200**, 21 (1992).
[20] L. X. Dang and B. C. Garrett, J. Chem. Phys. **99**, 2972 (1993).
[21] D. E. Smith and L. X. Dang, J. Chem. Phys. **100**, 3757 (1994).
[22] L. X. Dang, Chem. Phys. Lett. **227**, 211 (1994).
[23] L. X. Dang and P. A. Kollman, J. Phys. Chem. **99**, 55 (1995).
[24] L. X. Dang, J. Am. Chem. Soc. **117**, 6954 (1995).
[25] L. X. Dang, J. Chem. Phys. **96**, 6970 (1992).
[26] L. X. Dang, J. Chem. Phys. **102**, 3483 (1995).
[27] W. L. Jorgensen, OPLS Force Fields. In The Encyclopedia of Computational Chemistry, Wiley, New York 1998.
[28] K. Jensen and W. J. Jorgensen, Chem. Theory Comput. **2**, 1499 (2006).
[29] C. J. Fennel, A. Bizjak, V. Vlachy, and K. A. Dill, J. Phys. Chem. B **113**, 6782 (2009).
[30] M. Druchok, V. Vlachy, and K. A. Dill, J. Phys. Chem. B **113**, 14270 (2009).
[31] R. Zangi, J. Chem. Phys. **136**, 184501 (2012).
[32] H. J. C. Berendsen, J. R. Grigera, and T. P. Straatsma, J. Phys. Chem. **91**, 6269 (1987).